DOI: 10.61782/fa.2025.0407

FORUM ACUSTICUM EURONOISE 2025

FLOW-ACOUSTIC COUPLING IN VORTEX WHISTLE

Muriel Amielh[1*] **Daniel Mazzoni**[1] **Yann Pley**[1]
Jean-Jacques Lasserre[2]
[1] Aix Marseille Univ, CNRS, Centrale Méditerranée, IRPHE UMR 7342, 13384, Marseille, France
[2] Dantec Dynamics AS, DK-2740 Skovlunde, Denmark

ABSTRACT

The acoustic source we study is a vortex whistle composed of three parts of geometry and dimension similar to that of a bottle. The device consists of a cylindrical cavity with a circular base, a single fluid inlet tangential to the base of the cylinder and a cylindrical fluid outlet downstream which is a cylinder with a radius smaller than that of the cavity. The fluid (here air) entering the cavity generates a circular motion in the cavity and in the downstream cylinder. This device produces a sound with a dominant frequency. The frequency of the sound is controlled by the fluid flow rate. The characterization of the fluid vortex is performed in air by stereo-PIV (Particle Image Velocimetry), a laser optical diagnostics, resolved temporally and spatially, combined with acoustic measurements by microphone. In the exit section of the whistle, the center of the vortex circulates with a precession motion. From a decomposition into eigenmodes of the velocity field, the contributions to this motion are specified. The directivity diagram is established by calculating the Rayleigh integral based on the measured velocity fluctuations. The coupling between the acoustic field and the flow dynamics is thus highlighted and analyzed.

Keywords: *aero-acoustics, dipole source, time resolved stereo-PIV, proper orthogonal decomposition.*

**Corresponding author*: *muriel.amielh@univ-amu.fr.*

1. INTRODUCTION

The Vortex Whistle (Vonnegut, 1954 [1]) is a device generating sound by rotating a vortex within a cylindrical section with a tangential inlet. Vonnegut was the first to explain that the sound frequency generated at the outlet of the device is proportional to the fluid flow rate. At the outlet of the device, the fluid movement becomes unstable and generates a vortex agitated by a precessional movement. This instability is the cause of the sound emitted and an empirical formula in which the sound frequency varies according to the inlet-outlet pressure gradient and the dimensions of the device was proposed. His experiments showed that the Vortex Whistle works equally well in air and water. In 1963, Chanaud [2] sought to demonstrate the relationship between the vortex generated by instability and the sound frequency. His experimental work allowed him to explain that the sound frequency is the same as the frequency of the vortex's precessional motion at the device's outlet. Both Vonnegut and Chanaud mentioned the importance of considering friction losses in order to establish a right relation between frequency and flow rate, this being taken into account through a fitting empirical parameter in the law proposed by Vonnegut.
In the 2000s, applications for the Vortex Whistle emerged. For example, in 2013, Di et al. [3] suggested using it as a flow meter, given that frequency varies linearly with flow rate. In 2016, the device began to be used as a spirometer for medical applications [4].
In 2020, Kristiansen et al. [5] proposed a model based on the conservation of angular momentum, including friction losses. This model predicts the frequency as a function of the flow rate and device dimensions. The agreement was obtained with experiments in air and water for two different Vortex Whistles, respectively. The vortex precession at the outlet section of the Whistle was quantified by velocity

measurements by PIV ($2D-2C$) associated to acoustics measurements by microphone in air. A technique of phase averaging was performed in order to reconstruct the temporal dynamic of the vortex since the PIV was performed at 10 Hz whereas the characteristic flow frequency is in the range $200-1500Hz$. Their experiments allow them to characterize the acoustic radiation of the source, which they find similar to that of a dipole, confirming the previous result of Chanaud [2].
The objective of the present study is to identify the main contribution of the flow dynamics to sound generation. The detailed characterization of the vortex at the Vortex Whistle outlet is performed in air by fast stereo-PIV (Particle Image Velocimetry, $2D-3C$), a laser optical diagnostic, resolved temporally and spatially, combined with acoustic measurements by microphone. The experimental setup is described in Section 2. The velocity and acoustics results are analyzed in Section 3. By considering the helicoidal movement in the two cylinders constituting the Vortex Whistle, some improvements of the model initially developed in [5] are proposed. A Proper Orthogonal Decomposition is performed on the velocity field in order to highlight the cyclic movement associated to the dominant frequency for a given flow rate (Section 4).

2. EXPERIMENTAL SETUP

The geometry of the Vortex Whistle is presented in (Fig. 1). The main core of the Vortex Whistle with air tangential inlet is in aluminum, it is quite long compared to those studied by [2] and [5] with a length-to-diameter ratio of $L_c/D_c = 3.5$ (Tab. 1). For the nozzle, designed in plexiglass, this ratio is $L_o/D_o = 3.0$. The sudden reduction between these two parts is characterized by a diameter ratio $D_c/D_o = 2.5$. The surface of the internal wall is considered smooth.

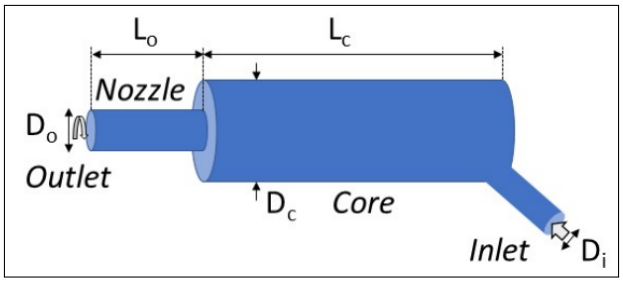

Figure 1. Geometry of the Vortex Whistle.

Table 1. Dimensions of the Vortex Whistle.

Geometry	Dimension
Inlet diameter, $D_i = 2R_i$	$14mm$
Outlet diameter, $D_o = 2R_o$	$20mm$
Oulet pipe length , L_o	$60mm$
Core diameter, $D_c = 2R_c$	$50mm$
Core length, L_c	$175mm$

Stereo-PIV images are acquired by a Dantec Dynamics system (RapiDO) that includes two T4040 SpeedSense Phantom high-speed cameras (2560×1664 $pixels$, 12 bits), and a double pulsed laser (Fig. 2). The pulsed laser is a Photonics laser (527nm, $2 \times 30mJ$ at a nominal 1kHz repetition rate). The DynamicStudio software controls synchronization of image acquisition. A laser sheet generator constituted of several suited lenses is installed at the end of the optical arm so that a flow field of $75.5 \times 49mm^2$ is illuminated. Stereo-PIV needs a depth calibration in order to correctly measure the U_z velocity component. This is performed with five calibration images of a motorized target positioned at $Z = 200\mu m$, $100\mu m$ and $0\mu m$, the laser sheet center. PIV images are acquired at a $4kHz$ rate and the time delay between two associated pulses is $5\mu s$. The flow is seeded by olive oil droplets of $2-3\mu m$ diameter introduced in the air circuit upstream the inlet of the Vortex Whistle.

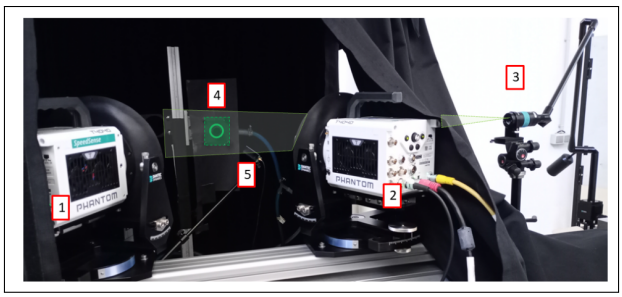

Figure 2. Set up of the nozzle outlet (4) flow investigation by high-speed stereo-PIV including two cameras (1 and 2), a laser sheet generator (3) and a microphone (5).

The spatial resolution is $\delta_x = \delta_y = 472\mu m$. The (O, X, Y, Z) coordinate system is centered on the exit cross-section on the nozzle where the investigation is fo-

cused. The three instantaneous components ($3C$) of velocity (U_x, U_y, U_z) are measured on the plane ($2D$) $Z = 0$ specified in (Fig. 2) by a green dotted line square. The velocity components in polar coordinates are (U_r, U_θ, U_z). 4000 instantaneous velocity fields are acquired for each flow conditions during $1s$. In the same time of PIV measurements, the acoustic pressure is measured by a microphone (1/4", GRAS) located at $(83mm, -63mm, 60mm)$ during $10s$ at a $25.6kHz$ sample frequency. Statistics and other post-processing on velocity fields and acoustic signals are performed by homemade codes developed in Matlab.

3. FLOW CHARACTERIZATION

The whistling is clearly detected by spectral analysis of acoustic pressure measured by microphone in the range $135 - 1200Hz$. Five flow conditions with velocity-pressure measurements are performed for the whistling frequencies $F_w = 135$, 410, 520, 620, 720 Hz. The flow rates q associated to these frequencies F_w are deduced from integration of the U_z velocity component over the exit cross-section of the nozzle. A summary of the flow conditions is given in Tab. 2.

Table 2. Flow conditions. $\tilde{U} = q/(\pi R_o^2)$, $\omega_o = 2\pi F_w$, $\overline{U}_z^* = \overline{U}_{z,max}/\tilde{U}$, $\overline{U}_\theta^* = \overline{U}_{\theta,max}/(\omega_o R_o)$, $S_w = \overline{U}_{\theta,max}/\overline{U}_{z,max}$.

F_w	$\tilde{U}$	$\omega_o R_o$	$\overline{U}_z^*$	$\overline{U}_\theta^*$	S_w
(Hz)	(m/s)	(m/s)			
135	2.15	3.92	1.48	0.474	0.583
410	12.5	25.8	1.58	0.523	0.682
520	15.3	32.8	1.59	0.500	0.674
620	18.0	39.0	1.57	0.500	0.689
720	19.8	45.2	1.58	0.473	0.684

Fig. 3 presents the mean velocity field at the section $Z = 0$. The rotating movement is in agreement with a tangential inlet located in the quarter ($X > 0, Y < 0$). In the outer region, for radius $R > 10mm$, the velocity vectors orientations highlight the external flow entrainment. This external part of the flow is not considered for the flow rate calculation.

The $\overline{U}_\theta$ (shown in Fig.4) and $\overline{U}_z$ mean velocity components are not maximum in the same regions of the flow,

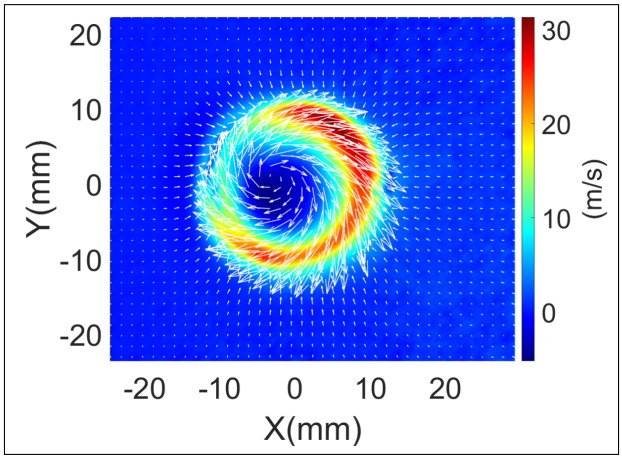

Figure 3. Mean velocity for $F_w = 720Hz$: ($\overline{U}_r$, $\overline{U}_{theta}$) vectors and $\overline{U}_z$ contours (see colorbar).

their maximum occur on rings centered on a radius of $8.3mm$ and $9.5mm$, respectively and independently of the flow conditions investigated here by PIV. In the quarter ($X < 0$, $Y > 0$) where $\overline{U}_z$ presents a minimum on its ring, it corresponds to a local maximum $\overline{U}_{\theta,max}$ of $\overline{U}_\theta$. The local maximum of $\overline{U}_z$ is named $\overline{U}_{z,max}$. Thus, the averaged velocity field is not axisymmetric. The similar non-dimensionalized values of $\overline{U}_\theta^*$ and $\overline{U}_z^*$ and of the swirl number S_w gathered in Tab. 2 for different F_w suggest a regime in similarity in the range $410 - 720Hz$.

Negative values of $\overline{U}_z$ in the center of this ring are significative of a flow reverse inside the nozzle due to the high level of swirl. The mean vortex center observed in Fig. 3 is in the region of negative $\overline{U}_z$. However, this mean position must be considered carefully, since actually, the instantaneous vortex follows a precession movement so that it is never at this position as shown in Fig. 5. The mean trajectory of the vortex center is shifted from the nozzle cross-section center and is located in the quarter ($X < 0, Y > 0$).

Thanks to the high speed PIV system, the instantaneous three velocity components are acquired at a sufficient high frequency in order to allow a right spectral analysis. Fig. 6 highlights the presence of the same predominant frequency in the velocity component signals extracted at the position ($X = 5mm$, $Y = 5mm$, $Z = 0mm$) than in the acoustic pressure signal measured by microphone according to the frequency resolution of 3.91 Hz for velocity and 1.56 Hz for acoustics. This

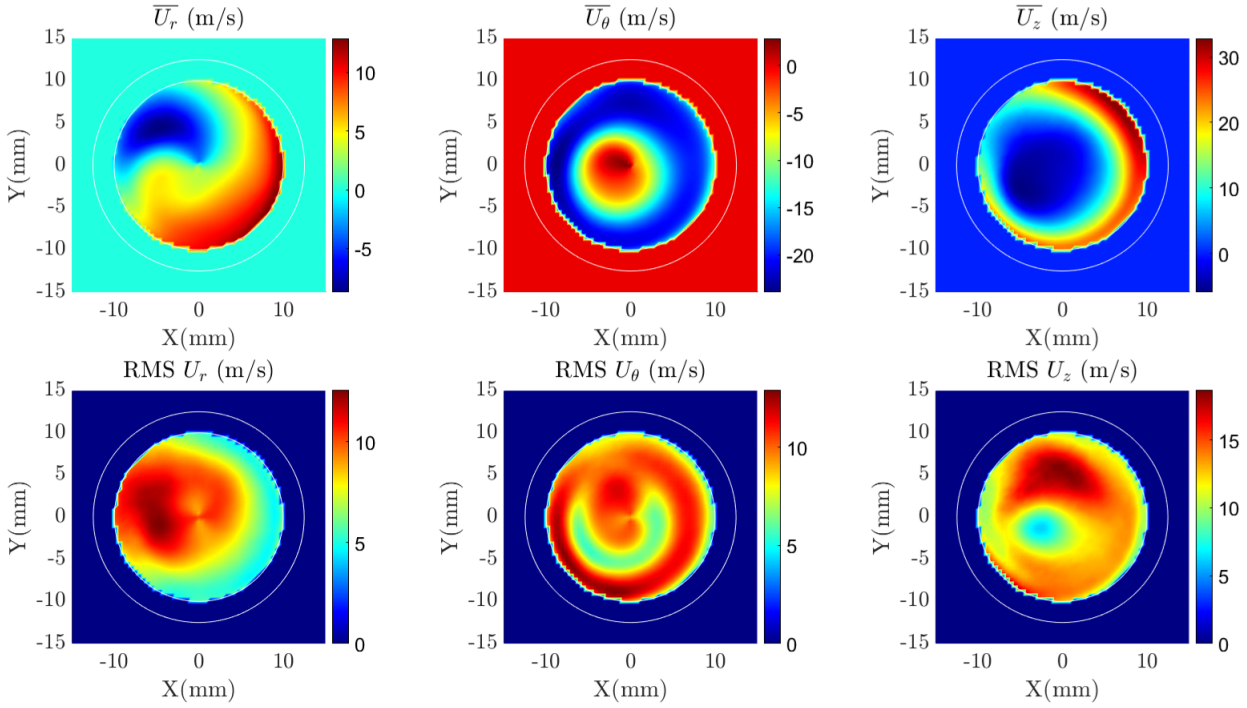

Figure 4. Velocity statistics in the exit cross-section of the nozzle from stereo-PIV measurements. Mean velocity components $\overline{(.)}$ (up) and velocity root mean square (RMS, down) for $F_w = 720Hz$.

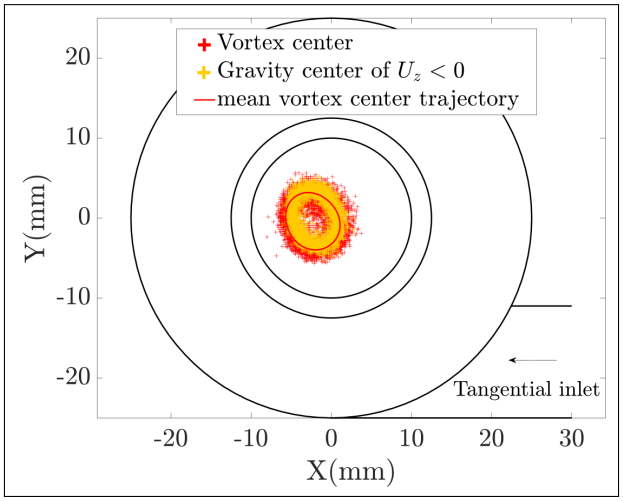

Figure 5. Instantaneous vortex and negative U_z region center positions detected from the 4000 PIV fields for $F_w = 720Hz$.

concordance is true in the whole velocity field and for all investigated flow rates.

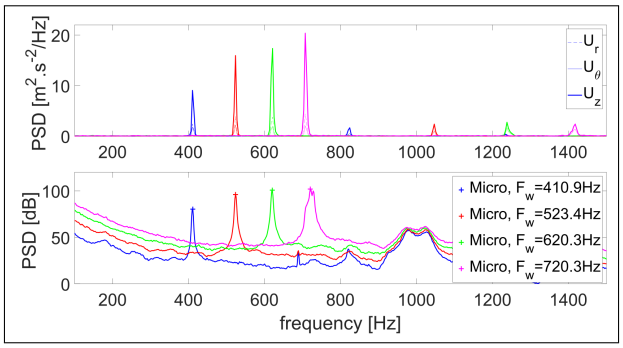

Figure 6. Spectral analyses of velocity components extracted at ($X_e = 5mm$, $Y_e = 5mm$, $Z_e = 0mm$) and pressure for different flow rates.

The linear dependency between flow rate q and whistling frequency F_w is confirmed as usually observed

for Vortex Whistle ([1, 2, 5]) as shown in Fig. 7. The model proposed by Kristiansen et al. [5] is compared with the present experimental results. Their relation between the whistling frequency F_w and the volume flow rate q was deduced from the balance of the kinetic momentum. The expression obtained without wall friction was :

$$F_w = \frac{q}{(\pi R_i R_o)^2}\,(R_c - R_i) \tag{1}$$

When considering the wall friction along the L_c and L_o lengths of the core and the nozzle respectively, the expression becomes:

$$F_w = q\frac{\sqrt{1 + 16\dfrac{(C_{F_c}L_c + C_{F_o}L_o)\,(R_c - R_i)}{R_i^2}} - 1}{8\pi^2\,(C_{F_c}L_c + C_{F_o}L_o)\,R_o^2} \tag{2}$$

where C_{F_c} and C_{F_o} are the friction coefficients in the core and the nozzle.

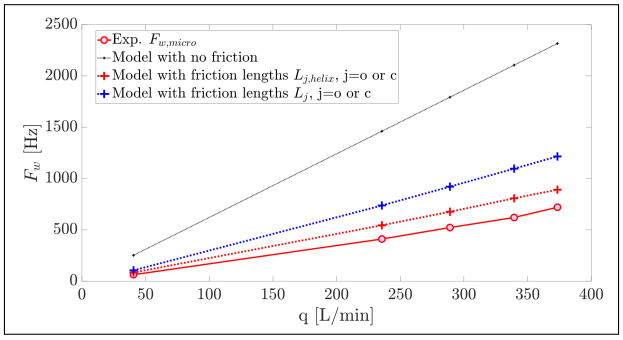

Figure 7. Whistling frequency vs flow rate. Adjustment of the model [5] by considering an elongation of friction length due to the helical movement inside the core and the nozzle.

While the model was in a good agreement with the results obtained by Kristiansen et al. [5] for Vortex Whistle with $L_c/D_c = 1.76$ and 1.94, the agreement is not so good with the present experimental results because the present frequencies are lower than those expected by the original model. The decrease of whistling frequencies for similar flow rate but with larger ratio length/diameter was also observed by Chanaud when varying L_o/D_o while keeping the same L_c/D_c. In the present experiment, the ratio $L_o/D_o = 3$ is smaller than those of the vortex whistles of Kristiansen et al. [5] where $L_o/D_o = 3.42$ and 3.85 while the D_i/D_c ratio are quite similar: respectively 0.28 here, and 0.30 and 0.26 for [5]. Thus, the lower experimental frequencies is not due to the variation of the parameter L_o/D_o, but probably to the larger ratio L_c/D_c = 3.5 for the present experiment. It means that friction is probably not sufficiently taken into account in the model. A proposed improvment of the model is to consider that a fluid particle will follow a helical trajectory both in the core and the nozzle, so that the friction length L_j ($j = o$ or c) to be considered in the model will become the length of the helix in each part of the Vortex Whistle by considering the translation velocity $q/\pi R_j^2$ and the rotation velocity $\omega_j R_j$:

$$L_{j,helix} = \frac{\pi R_j^2 L_j \sqrt{(\frac{q}{\pi R_j^2})^2 + \omega_j^2 R_j^2}}{q} \tag{3}$$

Results presented in Fig. 7 show a better agreement with this proposed model, but some differences remain, that can not be fully solved with this simple model.

4. FLOW FOOTPRINT ON ACOUSTICS

4.1 POD of the velocity field

In order to typify the effect of flow fluctuations on acoustics, the coherent structures that contribute to the dynamics are sought. The POD (Proper Orthogonal Decomposition) [6] is a right tool for the analysis of the fluctuating part of the velocity field. The POD principle is based on the decomposition on a basis of eigen modes sorted by their energetic contribution to the quantity of interest, here the velocity components. The decomposition is performed on 4000 uncorrelated snapshots of the three velocity components (U_r, U_θ, U_z), which determines a number of modes equal to the number of realizations. The interest is here focused on the ten first energetic modes.

Fig. 8 illustrates the cumulative energy for modes 1 to n when non-dimensionalized by the cumulative energy for mode 1 up to mode 10. When considering the cumulative energy of the two first modes (condition named POD [1 2] in Fig. 9 for e.g.), almost 50% of the cumulative energy of the 10 first modes (POD [1 ... 10]) is reached.

A spectral analysis made on the U_z signal extracted at the position ($X_e = 5mm$, $Y_e = 5mm$, $Z_e = 0mm$) from the PIV field measured for $F_w = 720Hz$ is presented in Fig. 9. The power spectral density (PSD) is compared with different POD reconstructed signals

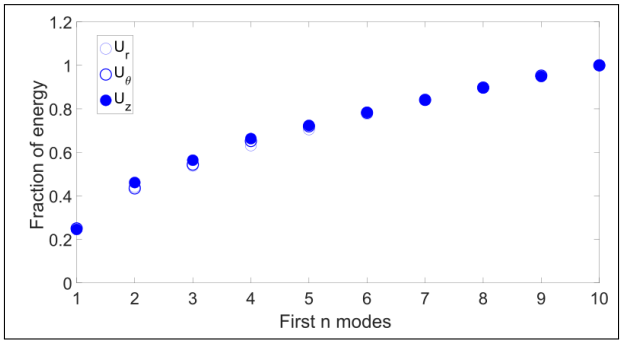

Figure 8. Fraction of energy captured by POD according to the ($n \leq 10$) considered modes for $F_w = 720Hz$.

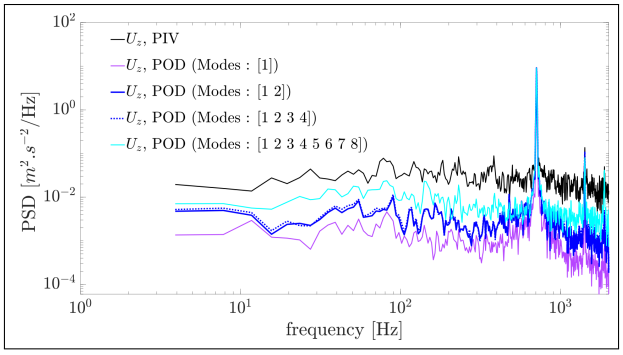

Figure 9. Spectral analysis of PIV and POD velocity signals at the position ($X_e = 5mm$, $Y_e = 5mm$, $Z_e = 0mm$) for $F_w = 720Hz$.

of U_z including only the first mode (POD [1]) up to eight modes ([POD [1...8]). For all the reconstructed POD signals, the predominant frequency F_w is preserved while the noise energy level is reduced. The energy related to the predominant peak is also respected since $PSD = 9.29m^2/s^2/Hz$ for the PIV and 9.16 and $9.11m^2/s^2/Hz$ for POD [1 2] and POD [1 2 3 4], respectively. Note that for POD [1] the PSD is only $3.88m^2/s^2/Hz$. Since no great difference in energy level is observed between the POD reconstructed PSD for POD [1 2] and POD [1 2 3 4], the rest of the following POD analyses will be based on the two first modes.

An example of velocity time series reconstitution by POD [1 2] at the position (X_e, Y_e, Z_e) is given in Fig. 10 (right) for the three velocity components (U_r, U_θ, U_z). The harmonic behaviour of the velocity signals is highlighted by POD while the phase is respected. In the left part of the figure is presented an instantaneous velocity field for (U_r, U_θ) where only one vector out of three is plotted for the sake of readability. The vector field obtained from POD is obviously smoothed and the instantaneous position of the vortex center is clearly detected.

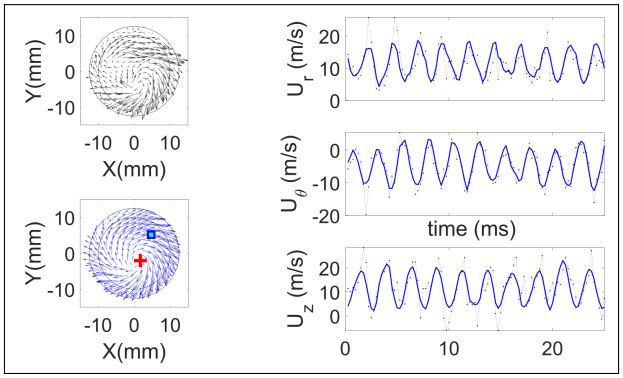

Figure 10. Comparison between PIV (black) measurements and POD analysis (blue) with the two first modes [1 2] for $F_w = 410Hz$. Instantaneous velocity vector (U_r,U_θ) at the exit cross-section of the nozzle (left). Extracted velocity signals (U_r, U_θ, U_z) at the position ($X_e = 5mm$, $Y_e = 5mm$, $Z_e = 0mm$) located by a blue square on the left figure (right). The red cross indicates the vortex center.

4.2 Directivity diagram

Since the signal $U_z(X, Y, Z, t = time)$ is available in the whole exit cross-section of the nozzle, the next step is to check if it is possible to estimate the acoustic pressure level and the directivity diagram from the POD [1 2] reconstruction. This estimation is performed by Rayleigh integral applied in the time domain, that can be written:

$$P(M,t) = \rho \iint_{\Sigma} \frac{1}{2\pi r_{MS}} \frac{dv_n(S, t - \frac{r_{MS}}{c})}{dt} dS \qquad (4)$$

where c is the sound speed, Σ is the source area and $v_n = U_z$ is the fluctuating velocity component normal to the exit cross-section of the nozzle. M is an observation point situated at a radius R_M from the center O of the nozzle exit section and at the angle ϕ where the contribution to the directivity diagram will be calculated. Fig. 11 illustrates the geometry for this pressure model. The red

radius is the location of the observation points M. dS (white square) is a surface element centered on the source point S located on the exit cross-section of the nozzle colored in blue in Fig. 11. The Rayleigh integral is calculated for $R_M = 0.5m$ using POD [1 2] reconstruction of U_z for $F_w = 410Hz$ and $720Hz$.

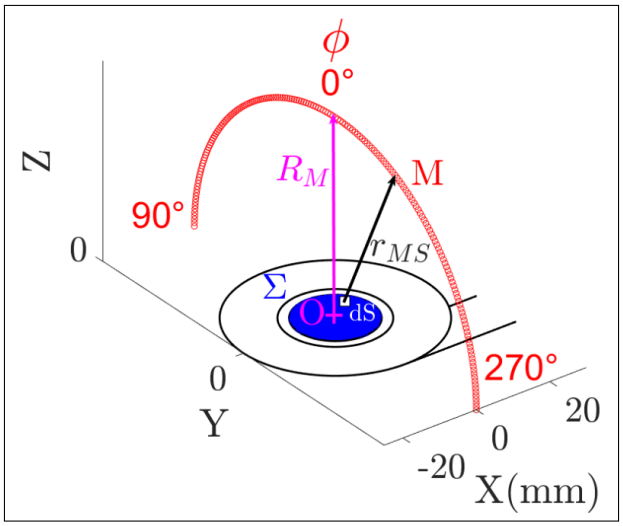

Figure 11. Angular positions of microphone (in red) for diagram directivity measurements.

The results are compared to measurements made at the same distance R_M with the microphone previously described (See Section 2) for three whistling frequencies $F_w = 606, 700$ and $725Hz$. For this experiment, the Vortex Whistle exit cross-section was installed flush with a rigid panel of large dimensions $1.5m \times 2.5m$. The results are presented as a directivity diagram in Fig. 12. The values of sound pressure level are overestimated by Rayleigh integral calculated with POD modes comparatively to experiments and no minimum is obtained at ϕ=0°. Contrariwise, such minimum of radiation at 0° angle, the main outlet flow direction, and larger values towards 90° and 270° are observed with experimental data, it could be associated to a dipole radiation as previously suggested by [2] and [5]. However the radiation is not symmetric against angles, a larger radiation is detected for the three experimental frequencies F_w in the angle range $300 - 330$, this is probably to be associated to the asymmetry of the real flow. Another proposed approach is to modeled the $U_z(R, \theta, z, t)$ by a sinus whose amplitude $A(R)$ is the radial profile of the experimental U_z root mean square deduced from PIV statistics post-process (See Fig.4), multiplied by $\sqrt{2}$. The proposed formulation is :

$$U_z(R, \theta, z, t) = A(R)\ sin(\omega_o\, t + \theta) \qquad (5)$$

The Rayleigh integral is calculated with this sinus model for $F_w = 720Hz$. A comparison between dU_z/dt calculated from POD modes or this sinus model is presented in Fig. 12 Due the symmetry of the sinus model, the typical radiation of a dipole is obviously obtained, but it is interesting to note that the maximum sound pressure levels are in good agreement with the experimental results as seen in the angle range 30-180°.

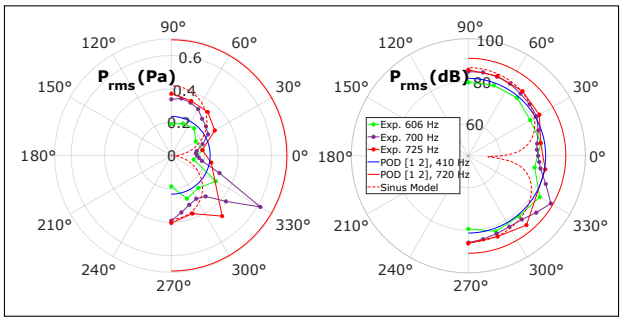

Figure 12. Directivity diagram in Pa (left) and in dB (right). The angle ϕ=0° corresponds to measurements on the axis on the outflow side.

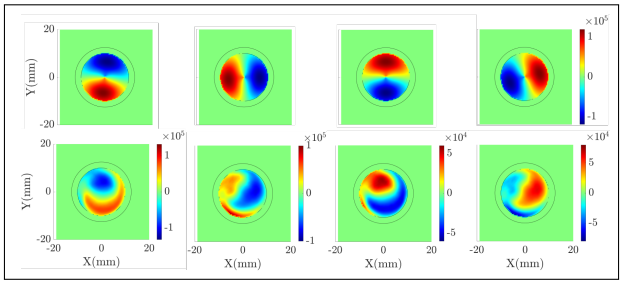

Figure 13. dU_z/dt with U_z estimated by sinus model (up) and POD (modes [1 2]) (down) for $F_w = 720Hz$ at four typical instants.

In order to check if acoustic radiation of the present experimental source embraces other characteristics of a dipole, one analyses the SPL level according to the whistling frequency. By considering that the sound power level Lw at distance R_S from the sound source, located in free field positioned over a rigid plane, can approximately

related to sound pressure level (SPL) by the relation:

$$Lw = SPL + 10log10(\frac{2\pi R_M^2}{S_0}) \quad (6)$$

where $S_0 = 1m^2$ and R_M is the radius of a large hemisphere enclosing the source, a study of the SPL will give some information on Lw. Fig. 14 illustrates the increase of SPL with the whistling frequency F_w for the acoustic pressure measured by microphone at the angle ϕ=30°. Comparisons are made with SPL calculated for the microphone signal filtered with a narrow pass-band filter around F_w and also with the SPL deduced from the Rayleigh integral on POD [1 2]. The typical slope 6 of a sound power level for a dipole is rather in a good agreement with the present results.

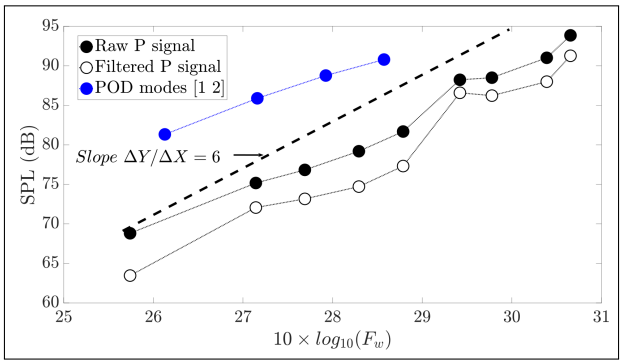

Figure 14. Sound pressure level *vs.* whistling frequency.

5. CONCLUSION

The flow dynamics in the exit section of a Vortex whistle was characterized by high-speed stereo-PIV velocity measurements combined with acoustic pressure measurements by microphone. Using POD, the spatio-temporal organization of the flow was highlighted. The main characteristics of Vortex Whistles previously studied in the literature were found, the dynamics of the velocity field and the acoustic pressure being interdependent. However, it seems that the length of the main cylinder influences the characteristics of the acoustic source that the Vortex Whistle simulates. If the acoustic levels and their radial distribution remain close to that typical of an acoustic dipole, the decentering of the precession movement seems to induce an additional complexity that a simple radiation model does not fully describe.

6. ACKNOWLEDGMENTS

The IRPHE technical staff is acknowledged for the design of the Vortex Whistle.
The high-speed stereo PIV system RapiDO is a funded project of A*Midex (Aix Marseille University).

7. REFERENCES

[1] B. Vonnegut, "A vortex whistle," *The Journal of the Acoustical Society of America*, vol. 26, no. 1, pp. 18–20, 1954.

[2] R. C. Chanaud, "Experiments concerning the vortex whistle," *The Journal of the Acoustical Society of America*, vol. 35, pp. 953–960, 1963.

[3] Y. Di, C. Gerhardy, and W. K. Schomburg, "Vortex whistles employed as remote micro flow sensors," *Flow Measurement and Instrumentation*, vol. 34, pp. 11–18, 2013.

[4] S. Kaiser, A. Parks, P. Leopard, J. C. Charlie Albright, M. Goel, D. Nassehi, and E. C. Larson, "Design and learnability of vortex whistles for managing chronic lung function via smartphones," in . *UbiComp '16*, (Heidelberg Germany), 2016.

[5] U. Kristiansen, M. Amielh, and D. Mazzoni, "On the sound production in vortex whistle," in *e-Forum Acusticum, 9th Edition*, (Lyon, France), 2020.

[6] G. Berkooz, P. Holmes, and J. Lumley, "The proper orthogonal decomposition in the analysis of turbulent flows," *Annual Review of Fluid Mechanics*, vol. 25, p. 539–575, 1993.